We are IntechOpen,
the world's leading publisher of Open Access books
Built by scientists, for scientists

6,900
Open access books available

186,000
International authors and editors

200M
Downloads

Our authors are among the

154
Countries delivered to

TOP 1%
most cited scientists

12.2%
Contributors from top 500 universities

Interested in publishing with us?
Contact book.department@intechopen.com

Numbers displayed above are based on latest data collected.
For more information visit www.intechopen.com

Analytical Model for Estimating the Amount of Heat Generated During Friction Stir Welding: Application on Plates Made of Aluminium Alloy 2024 T351

Miroslav Mijajlović and Dragan Milčić

Additional information is available at the end of the chapter

1. Introduction

Two decades after its invention, friction stir welding (FSW) has the status of a novel and promising welding technique that has not yet been fully described, investigated or utilized in industry [1]. It is a process of joining two metals/alloys, with relatively simple equipment, that initializes complex physical processes in/around the parts that are being joined, resulting in the monolith structure of these parts.

FSW is a patented [2-4] solid state welding technique that needs no consumables or shielding gasses (except in some special cases) for the creation of a welded joint. Welding is performed with a specialized, usually cylindrical, welding tool which mounts into the spindle of a machine that can rotate the tool around its axis (Fig. 1, a).

During the last few years, FSW has been standardized for the welding of aluminium [6, 7] and its principle of operation has been fully described for single welding tool application [7]. Welding parts (recognized as a base metal, workpieces) mount on the backing plate (anvil) [7] and rigidly clamp in such a manner that abutting or dilatation of the base metal is prevented. The rotating welding tool is inserted into the base metal by (axial) force at a start point on the joint line and travels along it [7]. While it travels, the welding tool "machines" material in the base metal in the zone near the traveling path and confines it in the working zone in a mixture that is deposed beside the welding tool as a weld. When the welding length is reached, the welding tool retracts from the base metal and welding is completed.
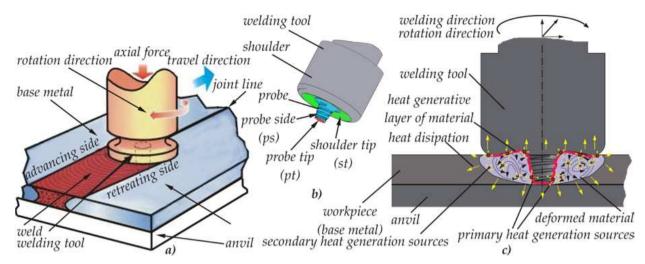
Figure 1. Schematic of FSW: a) principle of operation, b) welding tool, c) schematic of heat generation during FSW [5]

2. Heat generation during FSW

During FSW, the welding tool (Fig. 1, b) slides over the base metal, stirring, deforming, and mixing it. The base metal, anvil, and welding tool increase in temperature due the influence of the welding tool on the base metal. This change in temperature is a sure sign of heat generation caused by frictional contact that takes place during the welding process.

Thermodynamics recognizes several different types of heat transfer from a hotter to a colder body [8, 9]. Both the heat transfer and heat as an energy type have been investigated for a number of cases. However, a challenge appears when heat generation occurs as a result of the contact of two bodies. Heat generation is a process of energy transformation that takes place when one form of energy transforms into heat [8, 9]. This transformation is complex and it depends on the nature of the contact between the bodies, delivered loads, what materials are in contact, the surroundings, movement of the bodies etc. [9, 10]. Heat generated during FSW is the product of the transformation of mechanical energy delivered to the base metal by a welding tool. The transition of mechanical energy from the welding tool to the base metal happens between these bodies [10, 11]. Understanding that heat generates when a metallic body receives an "energy boost" and recognizing the dominant physical processes involved in the contact between the welding tool and base metal (friction, wear, adhesion, deformation, recrystallization of material, etc. [5, 11]), some might say that heat during FSW is primarily generated due to friction and deformation processes that appear during FSW [11]. Friction processes always appear in boundary layers and, therefore, the frictional heat generates in the boundary heat generative layer. Deformational heat appears wherever the deformation of base metal appears: in the boundary layer as well as in zone of deformed material around the welding tool [5, 11-13]. Heat generates due to other processes (e.g. infrared radiation, vibrations) but at a much lower intensity than results from friction and deformation.

Mechanical energy primarily transforms into heat when the welding tool contacts the base metal, while secondarily it transforms in deformed material around the welding tool (Fig. 1,

c). That is the reason why the heat generative layer is the primary heat generation source while deformed material around the welding tool is the volume of material where secondary heat generation sources appear [5]. Understanding the process of heat generation and estimating the amount of heat generated during FSW are complex and challenging tasks that requires a multidisciplinary approach. Estimating the amount of heat generated during FSW aids in understanding the appearance of thermal stress and structural changes in base metals inflicted by heat. Understanding the heat generation in FSW might help in selecting the optimal technological parameters of FSW (e.g. rotation frequency, travel rate) from aspects of minimal thermal stresses and deformations, energy consumption etc.

2.1. State of the art

Heat generation and heat transfer became a topic of research related to FSW during mid 1990s. However, understanding heat generation and heat transfer processes within FSW requires understanding several other physical processes: material flow around the welding tool, contact pressure inflicted by the welding tool, the friction coefficient, wear, change of thermo-mechanical properties and heat transfer coefficients etc. Nandan et al. [14] gives a review of thermal processes in FSW, from the invention of FSW until 2008.

Chao and Qi [15] have introduced a 3-D heat transfer model in FSW with constant heat input. Constant heat flux at the shoulder of the welding tool, constant contact pressure and pure Coulomb's friction law for estimating shear stress, and heat were the main assumptions of the model. The experimental welding of plates made of aluminum alloy 6061-T6 was performed and the temperature history of welding plates was estimated. Heat input was adjusted ("trial and error" principle) until numerical and experimental temperatures were matched. As such, this model is the first model developed for estimating the amount of heat generated during FSW. Frigaard and Grong [16] presented a process model for heat flow in FSW, where they assumed that heat is generated only by friction on the tops of shoulders and probes. Heat input and friction coefficients were adjusted during the welding process to keep the calculated temperature below the melting point of base metal material. Heat input was a moving heat source with a linear distribution of heat flux at the contact surface. Gould and Feng [17], and later Russell and Shercliff [18], have applied the Rosenthal equation [19] for describing the moving heat source, heat flux distribution, and heat transport within base metals, welding tools and the surrounding area. Models consider friction heat only at the shoulder and use a finite difference method for a numerical solution of the heat equation. Russell and Shercliff [18] based the heat generation on a constant friction stress equal to the shear yield stress at elevated temperature, which is set to 5% of the yield stress at room temperature. The heat input is a pure point or line source. Colegrove et al. [20] have used an advanced analytical estimation of the heat generation on the welding tool with a threaded probe to estimate the heat generation distribution. The results show that the fraction of heat generated by the probe is about 20% of the total amount. Shercliff and Colegrove [21] developed a material flow model that investigates the influence of threads on the probe on material flow. An advanced viscous material model is introduced and the influence of different contact conditions prescribed as the boundary

condition is analyzed. A thorough presentation of analytical estimates of the heat generation in FSW and influence of material flow on heat generation is given, as well. Khandkar et al. [22] introduced a torque based heat input model where experimentally estimated torque is a heat source. Khandkar modeled advanced heat transfer within the FSW process with frictional and deformational heat input into the process. Song and Kovačević [23] investigated the influence of the preheating period on the temperature fields in FSW. A sliding condition of the welding tool over the base metal was assumed and an effective friction coefficient and experimental plunge force are input into the heat source expression. Schmidt and Hattel [12] have defined an analytical model for estimating the amount of heat generated during FSW that recognizes the shoulder and the probe of the welding tool as heat sources and concludes that about 89% of heat is generated at the shoulder. Heat has friction and deformation components and the total heat is a sum of both with influence of the contact state variable [12, 24]. The effective value of the friction coefficient was used in calculations. Reliability of the previously proposed ideas and principles of heat generation were summarized by Nandan et al. [25]. Nandan has performed FSW of dissimilar aluminum alloys and his results have shown that a constant state variable (also referred as an extent of slip) gives values close to sticking.

Further advances in heat generation and modeling included finite element analysis (FEA) in FSW. Ulysse [26] presented a 3-D visco-plastic FEA model using the commercial software FIDAP. The heat generation was determined to be a product of the effective stress and the effective strain-rate. Results show that the model consistently over predicted the measured temperatures probably from an inadequate representation of the constitutive behavior of the material used in FSW. Steuwer et al. [27] used the experimentally observed mechanical power as input in the model. The influence of tool loads on residual stresses was investigated. Chao et al. [28] recognizes two boundary value problems in heat transfer: heat transfer in the welding tool as steady state while considering heat transfer within workpieces as transient. The amount of the heat that flows to the tool dictates the life of the tool and the capability of the tool in the joining process. In discussions, it is shown that the majority of the heat generated from the friction, about 95%, is transferred into the workpiece and only 5% flows into the tool and the fraction of the rate of plastic work – deformation, dissipated as heat is about 80%. Heurtier et al. [29] presented a 3-D model based on the fluid-velocity fields where the tool shoulder and the plastic strain of base material near the welding tool were heat sources. The model has shown good agreement regarding the numerical and experimental results. Santiago et al. [30] introduced a model with rigid and visco-plastic materials in which the plates move towards the rotating tool and the material flow at the interface is specified as a boundary condition. The results estimated from the model correspond to the steady state of the FSW process that has been proposed by Chao [28]. Schmidt [31] has adopted a fully coupled thermo-mechanical dynamic analysis model also aiming to achieve the steady welding state in ABAQUS/Explicit.

Colligan [32] gave a conceptual model that describes dominant parameters affecting heat generation including a detailed description of the existing literature and the principles of specific physical processes in FSW, e.g. friction coefficient. Kalya et al. [33] investigated

torque, specific energy and temperature during FSW and gave a correlation between torque, angular frequency and travel rate. The conclusion was a simple correlation between the friction coefficient and mathematically modeled torque. Kumar et al. [34] proposed an experimental setup for estimating the friction coefficient for different contact pressures, temperatures and materials of workpieces. A number of results showed that the friction coefficient varies during FSW from 0.1 up to 4. Setup and the mathematical model are limitedly applicable due to the design of the setup, kinematical complexity of the FSW and approximations involved in the mathematical model. Colligan [35] has investigated the material flow around the welding tool using a tracer embed and "stop action" technique. The results gave deep insight in the material flow patterns, influence of the thread on material flow, influence of rotation direction, as well as some metallurgic and details about heat transport in the zone of the deformed material. Nandan et al. [36] gave some numerically estimated results about viscoplastic material flow, heat transport, viscosity changing and material deposition behind the welding tool. Ouyang and Kovačević [37] have shown that material flow is always dissimilar along the joint line when welding either similar or dissimilar materials. Material flow-patterns can be easily traced in the vortex-like microstructure known as the welding nugget. Material in the zone of the nugget suffers significant plastic deformation, thermal recrystallization and acts like a quasi heat source. Lorrain [13] has explained in detail the shear layer of material and material flow patterns around the unthreaded probe. The existence of the rotating layer in the material near the welding tool is pointed out and it is concluded that material flow is significantly lower when a welding tool without threads is used. Lack of material flow had no influence of the strength of the weld.

2.2. Analytical model for estimating the amount of heat generated during FSW

Heat generation is an unavoidable process following the friction stir weld-creation process. Since FSW is a welding procedure that uses a welding tool as an initiator of the joining process of workpieces, the welding tool delivers activation energy [38, 39] to workpieces and the joining of the workpieces is achieved while heat generates.

This study presents an analytical model for estimating the amount of heat generated during FSW [5]. The model recognizes geometrical, kinematic, physical and energetic possibilities of heat generation during FSW, recognizes dominant parameters affecting the heat generation process and uses them to estimate how much mechanical power is transformed into heat. Existing models for estimating the amount of heat generated during FSW [12, 15, 17, 20, 22, 23, 25, 26] recognize many parameters affecting the heat generation process. Some of them are topology and geometry of the welding tool, technological parameters (tool rotation speed n [rpm] or angular velocity ω [rad/s], travel rate v_x [mm/s], tilt angle, etc.), loading (axial force F_z, torque M_t etc.), physical phases of FSW, duration of the welding procedure, duration of certain phases of the welding procedure, etc. Furthermore, these parameters initiate other parameters that affect heat generation process: friction coefficient μ, contact pressure p, shear stress τ, temperature T, mechanism of heat generation (defined

over e.g. the constant state variable δ), etc. However, presented models simplify FSW assuming e.g. constant friction coefficient [12], constant contact pressure [15], pure frictional heat generation [12, 15, 17, 23], heat generation only due work of the largest part of the welding tool [20, 23, 25, 26], no heat generation when temperature in the workpiece reaches melting point [22, 23] etc. Such assumptions are affecting the usability and the precision of results derived by developed models.

The model presented here considers many of the previously analyzed parameters. Special care in the model is given, beside estimating values of parameters, to the mutual dependences between parameters and their influence on the heat generation process. Such dependences are numerous and it is not possible to recognize all of them. Furthermore, many of them are too difficult to be explained analytically and require the numeric calculations and the experimental estimation/validation. These are the reasons why analytical model considers only the most important dependences (Fig. 2, a).

Because of the nature of this approach, the proposed analytical model relies on three major elements: analytic algebra, numerical calculations and experimental data [5]. The analytic algebra is based on existing research and results but includes some improvements. The algebra is developed for a complete welding tool, involves more dominant parameters in the calculations than in previous models, recognizes more dependencies between parameters, neglects fewer parameters and has a shorter calculation time. One of the improvements of the algebra is the implementation of a numerical material flow model with respect to energy balance in workpieces. The numerical calculations use adequate numerical procedures to give good precision and convergence during a short-computing time.
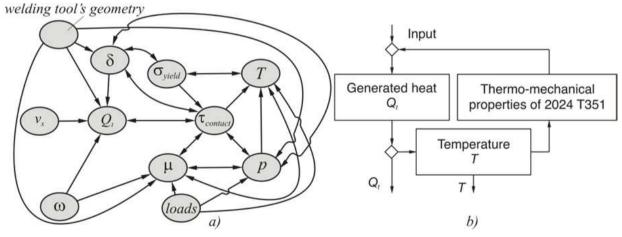

Figure 2. a) Schematic of mutual dependencies between generated heat and dominant influencing parameters [5, 44], b) Partial algorithm for generated heat estimation [5]

The analytical model gives precise results only if experimentally estimated parameters are involved in the model. Furthermore, verification of the analytical model can be done by comparing the results from analytical model with experimentally estimated results. Experimental data is obtained during the welding of the workpieces made of Al alloy 2024 T351 and is used as input and for verification of the analytical model. Mutual dependences of the parameters affecting the heat generation are derived in iterative work regime of the

analytical model: time and space are discretized and conditions numerically estimated for the present discretized moment of time are the input for the future discretized moment of time (Fig. 2, b).

Since welding tool is the main initiator of the welding and the heat generation process, it s important to analyze the welding tool and its influence on workpieces as well as the physical engagement of the welding tool while welding.

2.2.1. Active surfaces, active surfaces engagement and physical phases of the FSW process

A number of different types of welding tools have been introduced from 1992 until the present [1, 40, 41]. They differ in shape, dimension, mechanical properties etc., and every tool is applicable to a specific material and limitedly applicable to some others. However, all welding tools have the same basics: they consist of at least one shoulder carrying at least one probe directly involved in welding. Recently advanced bobbin tools [7] have appeared when the welding tool has two shoulders. No matter how complex or simple the welding tool is, a limited portion of the welding tool is in constant contact with the base metal and performs the welding. The welding contact region (WCR) on the welding tool consists of three areas called the active surfaces of the welding tool (ASWT). There are always three of them: probe tip (pt), probe side (ps) and shoulder tip (st) (Fig. 1, b). Complete welding and all physical processes following it appear on these surfaces or close to them [5]. Probe tip is usually the smallest ASWT located at the top of the probe. It can be flat, curved or flanged, and rounded at the corner where it connects with the probe side. The probe side is cylindrical or conned ASWT sharing the same rotational axis with the probe tip. The area of the probe side is enlarged by various threads or flanges that help in more intensive mixing of material into the weld [41]. The root of the probe side connects with the shoulder. The shoulder tip is the largest ASWT, usually flat or curved in a manner that creates a "reservoir" for flashed material that come from the workpieces. It is confined to the top surface of the weld and has a role in imperfection-free weld creation [11].

At the beginning of the FSW process, the welding tool is positioned above the workpieces and the rotation axis of the welding tool is (nearly) perpendicular to the joint line.

After positioning, the welding tool starts to rotate at a constant rate (n revolutions per minute, angular velocity of ω [rad/sec]) and slowly plunges into the workpieces in the direction of the $-z$-axis. That is the start of the welding process starts $t=t_0$. Plunging stops when the plunging depth is reached ($t=t_1$, duration of the plunging is $t_{pl}=t_1-t_0$). The plunging depth is equal to the height of the workpieces or slightly smaller and it is achieved at a constant travel rate of the welding tool of v_z. The welding tool continues to rotate and dwells until $t=t_2$. During this time period ($t_{dw1}=t_2-t_1$) the workpiece material is being prepared for the welding: it heats and softens in the area near the welding tool. Afterwards the welding tool begins a translational movement along the joint line (x-axis) at a constant travel rate of v_x. The rotation and translation of the welding tool make the workpiece material (near the welding tool) deform, stick and mix into a monolith composition (weld) that is deposed in the area behind the welding tool. Movement of the welding tool along the joint line lasts

until the welding length l is reached, at $t=t_3$. This period ($t_w=t_3-t_2$) is the productive phase of the welding process. Translation of the welding tool stops and the tool dwells at the end point until $t=t_4$ ($t_{dw2}=t_4-t_3$). The welding tool then moves in z direction and leaves the weld and workpieces. When the welding tool is completely removed from the workpieces ($t=t_5$, $t_{po}=t_5-t_4$) the welding process is over. The physical phases of FSW are shown in Fig. 3. In certain circumstances, dwelling can be excluded from the welding process, however, a full FSW process consist of the plunging phase (t_0 to t_1), first dwelling phase (t_1 to t_2), welding phase (t_2 to t_3), second dwelling phase (t_3 to t_4), and pulling out phase (t_4 to t_5) [5].
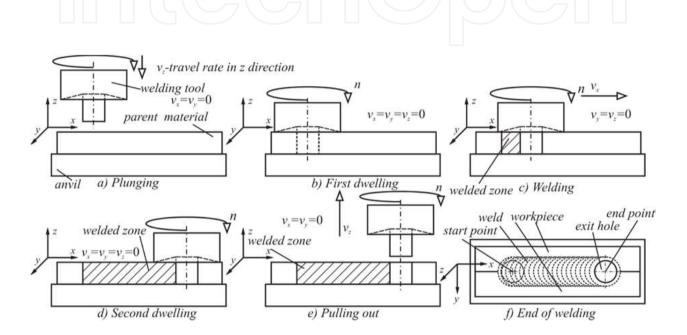

Figure 3. Physical phases of the friction stir welding process

Active surfaces of the welding tool are involved differently in the welding process during a complete cycle of welding, and engagement of every active surface varies during the cycle (Fig. 4, b). The probe tip is involved in welding from the beginning of the welding process until the end of the second dwelling phase (t_0 to t_4). Since the complete probe tip is fully involved in welding, engagement of the probe tip is considered as maximal. The probe side is involved in the welding process when intensive plunging appears (at $t_{pl'}$)[5, 42-46]. Engagement of the probe side rises with the rise of the probe plunge into workpieces. With the end of the plunging phase (t_1), engagement of the probe side reaches a certain value and keeps it during the complete first dwelling phase. When the welding phase starts (at t_2), engagement of the probe side rises toward maximal. This value is reached when the welding process stabilizes – travel rate (s) v_x reaches a steady value (at $t_{pl''}$) and it keeps constant until the end of the second dwelling phase (t_4) and afterwards it decreases. The shoulder tip is involved in the welding process before the end of the plunging phase (t_{st}) and it reaches full engagement when plunging stops (t_1) and keeps it until the end of the second dwelling phase.
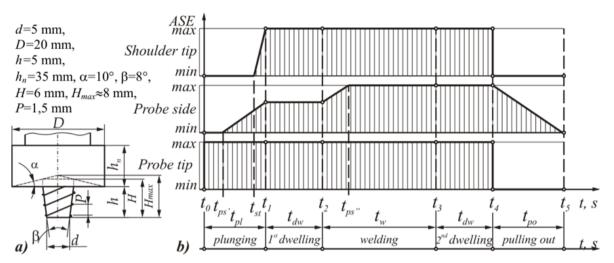
Figure 4. a) Welding tool used for experiments [5], b) Active surface engagement (ASE) [44]

2.2.2. Estimating the amount of heat generated during FSW

As previously mentioned, the heat generation process within FSW is a process that transforms mechanical energy (power) into heat. If η_Q represents a heat transformation [5], the total amount of heat generated during FSW - Q_t is a function of mechanical power P_a delivered to the welding tool:

$$Q_t = \eta_Q P_a \text{ [W]}, \quad \eta_Q = (0, 1) \tag{1}$$

The welding tool performs dual movement: translation (tr) and rotation (rot), and the total amount of generated heat is the sum of translation Q_{ttr} and rotational-generated heat Q_{trot}:

$$Q_t = Q_{ttr} + Q_{trot} = Q_{ttr}^{\;\;0} + Q_{trot} \tag{2}$$

The amount of translation heat is significantly smaller than amount of rotational heat [5, 12] and it can be neglected in analysis.

Heat is generated at or near the ASWT [5, 10, 12] and the total amount of generated heat is the sum of heat generated on every ASWT:

$$Q_t = Q_{pt} + Q_{ps} + Q_{st} \tag{3}$$

where Q_{pt} – the amount of heat generated at probe tip, Q_{ps} – the amount of heat generated at probe side and Q_{st} – the amount of heat generated at shoulder tip.

Simplifying the analysis and assuming that the total amount of mechanical power transforms into heat ($\eta_Q = 1$), the total amount of heat becomes:

$$Q_t = Q_{tr} = P_a \tag{4}$$

Mechanical power depends on angular frequency ω and torque M_t and the total amount of generated heat is:

$$Q_t = \omega M_t \tag{5}$$

and

$$\mathrm{d}Q_t = \omega\mathrm{d}M_t = \omega r\mathrm{d}F_t = \omega r\tau_{cont}\mathrm{d}A \tag{6}$$

where $\mathrm{d}F_t$ - infinitesimal force, r - distance of a infinitesimal segment, $\mathrm{d}A$ - infinitesimal area, τ_{cont} - contact shear stress in material.
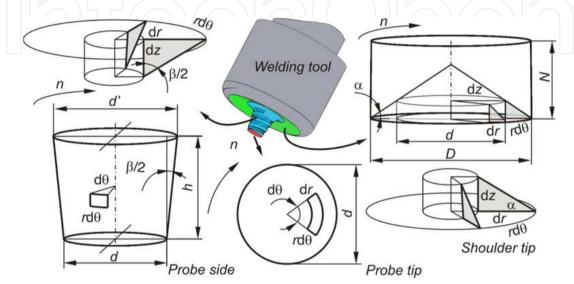

Figure 5. Active surfaces of the FSW welding tool

Different topologies of active surfaces result in different amounts of heat generated on them that give different expressions for estimating the amount of generated heat (Fig. 5). After the integration of Eq. 6, the expressions for the analytical amount of heat generated on every ASWT are, respectively:

$$Q_{pt} = \int\limits_0^{2\pi}\int\limits_0^{d/2} \omega r^2\tau_{cont}\mathrm{d}\theta\mathrm{d}r = \frac{2}{3}\pi\omega\tau_{cont}\left(\frac{d}{2}\right)^3 \tag{7}$$

$$Q_{ps} = \int\limits_0^{2\pi}\int\limits_0^{h} \omega\left(\frac{d}{2}\right)^2\tau_{cont}\left(1+\mathrm{tg}\frac{\beta}{2}\right)\mathrm{d}\theta\mathrm{d}z = 2\pi\omega\tau_{cont}\left(\frac{d}{2}\right)^2 h\left(1+\tan\frac{\beta}{2}\right) \tag{8}$$

$$Q_{st} = \int\limits_0^{2\pi}\int\limits_{d/2}^{D/2} \omega r^2\tau_{cont}\left(1+\tan\alpha\right)\mathrm{d}r\mathrm{d}\theta = \frac{2}{3}\pi\omega\tau_{cont}\left[\left(\frac{D}{2}\right)^3 - \left(\frac{d}{2}\right)^3\right]\left(1+\tan\alpha\right) \tag{9}$$

where: d - nominal diameter of probe, D - diameter of shoulder, h - height of probe, α - cone angle of shoulder, β - cone angle of probe.

There is heat generated by friction (frictional heat) and heat generated by deformation (deformational heat) [5, 10-12]. Both types of heat appear simultaneously on every ASWT and both influence one another. Considering both types of heat and their mutual influence

on one another, the total amount of heat generated on the probe tip, probe side, and shoulder tip are, respectively:

$$Q_{pt} = \left(1 - \delta_{pt}\right)Q_{pt}^{fr} + \delta_{pt}Q_{pt}^{def} \tag{10}$$

$$Q_{st} = \left(1 - \delta_{st}\right)Q_{st}^{fr} + \delta_{st}Q_{st}^{def} \tag{11}$$

$$Q_{ps} = \left(1 - \delta_{ps}\right)Q_{ps}^{fr} + \delta_{ps}Q_{ps}^{def} \tag{12}$$

where heat indexed with *fr* represents frictional heat, heat indexed with *def* represents deformational heat, δ_{pt}, δ_{ps}, δ_{st} – a dimensionless contact state variable (extension of slip) at the probe tip, probe side and shoulder tip, respectively.

The frictional and deformational amount of heat in equations 10, 11 and 12 for every ASWT, using Equations 7, 8 and 9 with respect to the contact shear stress [12, 5] is:

$$\tau_{cont} = \begin{cases} \mu p & \text{, for frictional heat generation} \\ \tau_{yield} & \text{, for deformational heat generation} \end{cases} \tag{13}$$

where: μ-friction coefficient, p-contact pressure, τ_{yield}-shear yield strength of workpieces.

Beside geometrical dimensions of the welding tool (d, D, h, H, α, β, etc.) and technological parameters of the process (ω, v_x), all other parameters (μ, p, τ_{cont}, τ_{yield}, T, $F_z(t)$, $M_t(t)$, δ_{pt}, δ_{ps}, δ_{st}, t_1, t_2, $t_{ps'}$, t_{st}, etc.) necessary for the analytical model have to be estimated analytically, numerically, experimentally or combining the estimation procedures.

Estimating the friction coefficient: Due to the complex kinematics of the FSW, it is difficult to establish a straightforward procedure for estimating the friction coefficient in FSW. Previous research recognizes the friction coefficient as a variable in FSW, but neglects the variation and assumes a constant value throughout the complete cycle of FSW. Usually, the friction coefficient within FSW, for a welding tool made of steel and workpieces of aluminium is equal to 0.3-0.4 [12, 34].

Kumar et al. [34] proposed an experimental model for estimating the friction coefficient during FSW. The model is based on the experimental estimation of the momentum of friction and axial force, which are necessary for estimating the friction coefficient. Figure 6 gives the functional schematic of the measuring place for the estimation of the friction coefficient. To estimate the coefficient of friction during FSW, it is necessary to estimate the momentum of friction and axial force [5]. The momentum of friction is the multiplication of the tangential force $F_t(t)$ (measured at force sensor 10, Fig. 6) and length of the pole (friction pole) L_t. If the diameter of the welding tools probe in contact is $d(t)$ and axial force is $F_z(t)$, the friction coefficient μ can be estimated as [14, 34]:

$$\mu = \frac{3F_t(t)L_t}{F_z(t)d(t)}, \quad t_2 \geq t \geq t_0 \tag{14}$$
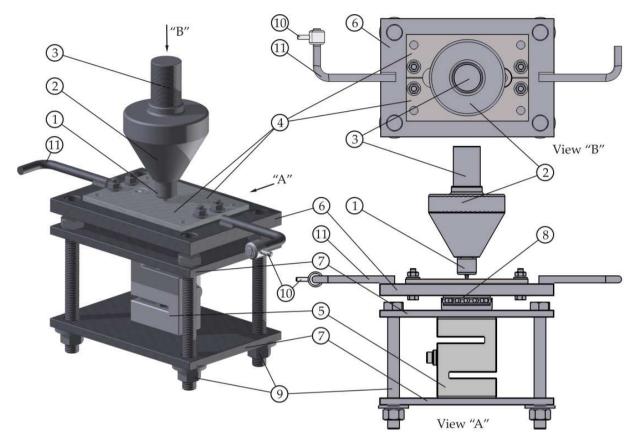
Figure 6. The measuring configuration for the momentum of friction and axial force: 1-welding tool, 2-welding tool's spindle, 3-shaft, 4-workpieces, 5-force sensor (axial force), 6-anvil, 7-backing plate, 8-ball bearing, 9-fundamental bolts, 10-force sensor (tangential force), 11-pole

The proposed model gives approximate results and only for the first two phases of FSW – plunging and first dwelling. The model is not applicable to the welding phase because the measuring system loses its stability when the welding tool travels along the join line and the momentum of friction cannot be measured [5]. Without proper model for estimating the friction coefficient during welding phase, friction coefficient has to be modeled. Friction coefficient used for the analytical model is estimated regarding the experimental results.

Estimating the contact pressure: Contact pressure p appears at the beginning of the plunging phase as a result of axial load $F_z(t)$ on the welding tool. Hertz [45] has proposed the first model for distributing contact pressure if a cylinder with a flat base punches into the plane, while Munisamy et al. [46] and Levytsky [47] have proposed models describing contact pressure distribution and heat generation when the axis of the cylinder is tilted.

Distribution of the contact pressure $p(r,t)$ delivered by the flat probe tip (Fig. 7, a) is [48]:

$$p(r,t) = \frac{2F_z(t)}{d\pi\sqrt{d^2 - 4r^2}}, \; t_0 \le t < t_{st}, \; 0 \le r \le \frac{d}{2} \tag{15}$$
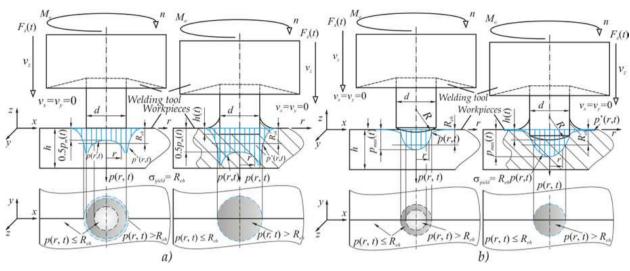
Figure 7. Contact pressure distribution for a) flat and b) spherical probe tips [4, 42, 43]

If the probe tip has a spherical shape, contact pressure is distributed (Fig. 7, b) as [48]:

$$p(r,t) = \frac{2}{\pi}\sqrt{d^2 - 4r^2}\sqrt[3]{\frac{3F_z(t)\overline{\overline{E}}^2}{d^5}}, \ t_0 \le t < t_{st}, \ 0 \le r \le \frac{d}{2} \tag{16}$$

where $\overline{\overline{E}}$ – represents the median modulus of elasticity estimated as:

$$\frac{1}{\overline{\overline{E}}} = \frac{1-v_{wt}^2}{E_{wt}} + \frac{1-v_{wp}^2}{E_{wp}} \tag{17}$$

and E_{wt} – the modulus of elasticity of welding tool's material, v_{wt} – the Poison's ratio of welding tool material, E_{wp} – the modulus of elasticity of the workpieces's material, v_{wp} – Poison's ratio of the workpieces's material.

For engineering practice median contact pressure $p_m(t)$ gives good results:

$$p \approx p_m(t) = \frac{4F_z(t)}{d(t)^2 \pi}, \ d(t) = d, \ t_0 \le t < t_{st}, \ 0 \le r \le \frac{d}{2} \tag{18}$$

Research [5, 10, 42-44] has shown that contact pressure distributed to workpieces reaches different values in different zones – in some zones it overcomes the yield strength of workpieces, while in other zones it has values lower than the yield strength (Fig. 8, c).

Existence of such zones multiplies the resistance of workpieces and plunging and intensive plunging appears when [5, 10, 42-44]:

$$p_m(t) > k_{eh}\sigma_{yield}(T); \ k_{eh} = 1.5\text{-}3 \tag{19}$$

where: $\sigma_{yield}(T)$ – yield strength of workpieces in function dependence with temperature T.
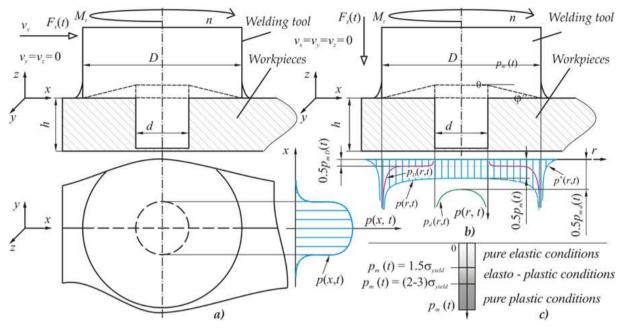
Figure 8. Contact pressure distribution [4, 42, 43]: a) probe side, b) shoulder tip, c) contact pressure defining contact conditions [5, 10, 42]

Contact pressure delivered by the shoulder tip is similarly distributed (Fig. 8, b) with a flat probe tip [5]. It appears smoothly since the shoulder tip is continuously involved in welding. Superposed contact pressure delivered by the probe tip and shoulder tip [5] is:

$$p \approx p_m(t) = \frac{4F_z(t)}{d(t)^2 \pi}, \quad d(t) \begin{cases} \approx \dfrac{d-D}{t_{st}-t_1} \cdot (t-t_{st})+d, \ t_{st} \leq t < t_1 \\ = D, \hspace{3.2cm} t_1 \leq t < t_4 \end{cases} \tag{20}$$

Contact pressure delivered by the probe side (Fig. 8, a) is a case of a modified "cylinder in cylinder" contact problem [45, 49]. Threads on the probe side increase the complexity of the analysis of the contact pressure distribution, however, with or without threads, median contact pressure on the probe side is:

$$p \approx p_m(t) \begin{cases} \approx \dfrac{F_x(t)}{dh}, \ t_2 < t < t_3 \\ \approx 0, \hspace{0.8cm} t \leq t_2, \, t \geq t_3 \end{cases} \tag{21}$$

where: $F_x(t)$ – force in welding direction, h – height of the probe/workpieces.

Estimating the tangential shear stress: When the deformation of workpieces appears, the rotational layer of the softened material travels around the welding tool [5, 12, 35, 37]. This is possible only if loads delivered by the welding tool inflict tangential stresses larger than the shear yield strength. The boundary value of such tangential shear (contact) stress, from von Misses yield criterion in uniaxial tension and pure shear [5, 12, 41, 42], is:

$$\tau_{cont} = \tau_{cont}(T) = \tau_{yield}(T,\varepsilon) = \sigma_{yield}(T,\varepsilon) / \sqrt{3} \tag{22}$$

where: $\tau_{cont}(T)$ – tangential contact stress in function of temperature T, $\tau_{yield}(T,\varepsilon)$ – shear yield strength of workpieces' material in function of temperature T and strain rate ε, $\sigma_{yield}(T,\varepsilon)$ – yield strength of workpieces' material in function of temperature T and strain rate ε. Yield strength of material is highly dependent on the temperature and strain rate, and the analysis of tangential stresses within FSW requires the full temperature and strain history in of the workpieces in a wide zone around the welding tool [5, 11, 14, 17, 23, 24, 27, 30]. However, analysis of heat generation in FSW can neglect the influence of strain on the decrease of yield strength and still maintain sufficient precision [12]. Neglecting is possible since the maximal temperatures of the material reach about 80% [38] of the melting temperature when strain has significant values due to near melting conditions in the material [18, 22]. Tangential contact shear stress is:

$$\tau_{cont} = \sigma_{yield}(T) / \sqrt{3} \tag{23}$$

where: $\sigma_{yield}(T)$ –yield strength of workpieces' material in function of temperature T. Thermo-mechanical properties of Al 2024 T351 are given in [5, 12, 50-53].

Estimating the contact state variable: The contact state variable or extent of slip is a parameter defining the influence of slipping in the heat generation process following the difference in the velocity of the welding tool and material, and relates frictional vs. deformational heat. It is obtained after curve fitting the experimental data regarding measured velocities [12, 14, 54, 55]:

$$\delta = \delta_{\min} + \left(1 - \delta_{\min}\right)\left(1 - e^{A_R}\right), \ A_R = -\delta_0 \frac{\omega r}{\omega_0 R} \tag{24}$$

where: δ_{min} – minimal measured slip, δ_0 – adjustable parameter depending on the material of the workpieces, R – maximal radius of the welding tool, ω_0 – normalized angular frequency of the welding tool (often the mid-point of the diapason of the measured angular frequencies).

Early works [12] considered the extent of slip as a single value for a complete welding tool. Experiments [5] have shown that the decomposition of the welding tool provides more precise results for the extent of slip if estimated for every ASWT separately. For example, when welding Al alloys with a steel welding tool with a threaded probe [12], with concern for the ASE of ASWT, the partial extent of slip is:

$$\delta_{pt} = \begin{cases} 0, & t_0 \le t < t_2, \ t_3 \le t < t_4 \\ \delta_{pt\ \min} + \left(1 - \delta_{pt\ \min}\right)\left(1 - e^{A_d}\right), \ A_d = -\delta_0 \dfrac{2\omega r}{\omega_0 d}, & t_2 \le t < t_3 \end{cases} \tag{25}$$

$$\delta_{ps} = \begin{cases} 0, & t_1 \le t < t_2, \ t_3 \le t < t_4 \\ \delta_{ps\ \min} + \left(1 - \delta_{ps\ \min}\right)\left(1 - e^{A_d}\right), \ A_d = -\delta_0 \dfrac{2\omega r}{\omega_0 d}, & t_{ps'} \le t < t_1, \ t_2 \le t < t_3 \end{cases} \tag{26}$$

$$\delta_{st} = \begin{cases} 0, & t_{st} > t \geq t_4 \\ \delta_{st\ min} + \left(1 - \delta_{st\ min}\right)\left(1 - e^{A_D}\right), A_D = -\delta_0 \dfrac{2\omega r}{\omega_0 D}, & t_{st} \leq t < t_4 \end{cases} \qquad (27)$$

where: $\delta_{pt} = 0.1$, $\delta_{ps} = 0.2$, $\delta_{st} = 0.1$, $\delta_0 = 0\text{-}1$ from [5].

Estimating the temperature history of workpieces: Estimation of workpiece temperature requires knowing how much heat is generated during welding since heat influences temperature increase and it has to be done in an iterative regime . An iterative regime requires the discretization of time and space (Fig. 9, b), numeric calculations and significant computing time [5]. Temperature history of workpieces and welding tool can be estimated solving heat equations:

$$\rho_w c_w \frac{\partial T}{\partial t} = \lambda_w \left(\frac{\partial^2 T}{\partial x^2} + \frac{\partial^2 T}{\partial y^2} + \frac{\partial^2 T}{\partial z^2} \right) + q_v \quad \text{(for workpieces)} \qquad (28)$$

$$\rho_{wt} c_{wt} \frac{\partial T}{\partial t} = \frac{\lambda_{wt}}{r} \frac{\partial}{\partial r}\left(r \frac{\partial T}{\partial r} \right) + \frac{\lambda_{wt}}{r^2} \cdot \frac{\partial}{\partial \varphi}\left(\frac{\partial T}{\partial \varphi} \right) + \lambda_{wt} \frac{\partial}{\partial z}\left(\frac{\partial T}{\partial z} \right) + q_v \quad \text{(for welding tool)} \qquad (29)$$

where: ρ_w – density of the workpiece, c_w – specific heat capacity of the workpiece, λ_w – thermal conductivity of the workpiece, ρ_{wt} – density of the welding tool, c_{wt} – specific heat capacity of the welding tool, λ_{wt} – thermal conductivity of the welding tool.
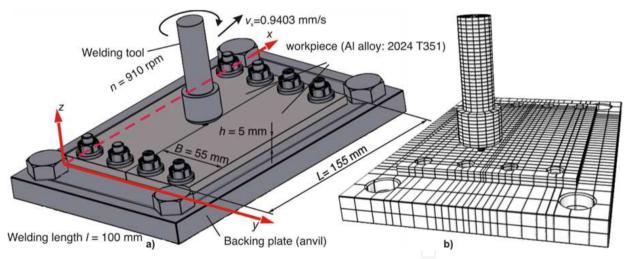

Figure 9. Workpieces, welding tool, bolts and anvil positioned for welding: a) realistic view with dimensions and some technological parameters used in experiment [5], b) discretized view (primarily and secondarily meshed with adaptive grid) [5]

Thermal energy generation source q_v is directly affected by generated heat Q_t and volume receiving generated heat V_t:

$$q_v = Q_t / V_t \qquad (30)$$

Initial conditions for such a system include the recognition of the initial temperature:

$$T(x, y, z, t_0) = T(r, \varphi, z, t_0) = T_0 \tag{31}$$

Boundary conditions are complex due to the complex geometry of the welding tool and complex kinematics. As an example, boundary conditions for the top surface of workpieces involve convective and radiation heat transfer:

$$\lambda_w \left(\frac{\partial T}{\partial z} \right)_{z=h} = \alpha \left(T_0 - T_{i,j,k} \right) + \sigma \bar{\varepsilon} \left(T_0^4 - T_{i,j,k}^4 \right) \tag{32}$$

where: α - heat transfer coefficient, σ - Stefan-Boltzmann constant, $\bar{\varepsilon}$ - thermal emissivity of workpieces, T_0 – ambient temperature.

Boundary conditions on the contact between workpieces and anvil:

$$\lambda_w \left(\frac{\partial T}{\partial z} \right)_{z=0} = \lambda_a \left(\frac{\partial T}{\partial z} \right)_{z=0} \rightarrow \lambda_w \left(\frac{\partial T}{\partial z} \right)_{z=0} = \alpha_{aprox} \left(T_{i,j,k} - T_0 \right) \tag{33}$$

where: λ_a – the thermal conductivity of anvil, α_{aprox} – approximated heat transfer coefficient.

Boundary conditions between the welding tool and workpieces involve conduction between the parts. Such condition is decomposed to a classical conductive boundary condition:

$$\lambda_w \left(\frac{\partial T}{\partial r} \right)_{r=d/2} = \lambda_{wt} \left(\frac{\partial T}{\partial r} \right)_{r=d/2} \tag{34}$$

and influence of heat transfer due to material flow [5]. The material of the workpieces in the welding zone travels around the welding tool and partially carries its energy balance with it. If analyzed in discretized space and during discretized time, nodes "travel" from one discretized position to another and they "carry" its temperature, and while traveling they get and lose a burst of heat. This model of material travel is based on research concerning material flow around the welding tool [5, 13, 14, 20, 25, 26, 30, 34, 37], and applied in numerical calculations of temperature and heat flow. The model is named "node substitution and replacement method - NSRM" [5].

Results can be obtained analytically and numerically – for temperature estimation, a finite difference method, an explicit scheme with an adaptive grid were used, with the application of algorithm NSRM. The numerical solution of Eqs. 29-30 with the application of Taylor series for approximation of 2nd order derives and node positioning in discretized space is:

$$T_{i,j,k}^{m+1} = \frac{\Delta t}{\rho_w c_w} \left[\lambda_w \left(K_{x"} + K_{y"} + K_{z"} \right) + q_v \right] + T_{i,j,k}^m \quad \text{(for workpiece)} \tag{35}$$

$$T_{i,j,k}^{m+1} = \frac{\Delta t}{\rho_{wt} c_{wt}} \left[\lambda_{wt} \left(\frac{K_{r'}}{r_i} + \frac{K_{\varphi"}}{r_i^2} + K_{z"} \right) + q_v \right] + T_{i,j,k}^m \quad \text{(for welding tool)} \tag{36}$$

where:

$$K_{x''} = \frac{T_{i+1,j,k}^m - T_{i,j,k}^m}{(x_{i+1} - x_i)(x_i - x_{i-1})} - \frac{T_{i,j,k}^m - T_{i-1,j,k}^m}{(x_i - x_{i-1})^2}, K_{y''} = \frac{T_{i,j+1,k}^m - T_{i,j,k}^m}{(y_{i+1} - y_i)(y_i - y_{i-1})} - \frac{T_{i,j,k}^m - T_{i,j-1,k}^m}{(y_i - y_{i-1})^2}, \quad \text{(a)}$$

$$K_{z''} = \frac{T_{i,j,k+1}^m - T_{i,j,k}^m}{(z_{i+1} - z_i)(z_i - z_{i-1})} - \frac{T_{i,j,k}^m - T_{i,j,k-1}^m}{(z_i - z_{i-1})^2}, K_{\varphi''} = \frac{T_{i,j+1,k}^m - T_{i,j,k}^m}{(\varphi_{i+1} - \varphi_i)(\varphi_i - \varphi_{i-1})} - \frac{T_{i,j,k}^m - T_{i,j-1,k}^m}{(\varphi_i - \varphi_{i-1})^2}, \quad \text{(b)}$$

$$K_{r'} \approx r_{i+\frac{1}{2}} \frac{T_{i+1,j,k}^m - T_{i,j,k}^m}{(r_{i+1} - r_i)(r_i - r_{i-1})} - r_{i-\frac{1}{2}} \frac{T_{i,j,k}^m - T_{i-1,j,k}^m}{(r_i - r_{i-1})(r_i - r_{i-1})}, \; r_{i+\frac{1}{2}} \approx r_i + \frac{r_{i+1} - r_i}{2}, \quad \text{(c)}$$

$$K_{r''} \approx \frac{T_{i+1,j,k}^m - T_{i,j,k}^m}{(r_{i+1} - r_i)(r_i - r_{i-1})} - \frac{T_{i,j,k}^m - T_{i-1,j,k}^m}{(r_i - r_{i-1})^2}, \; r_{i-\frac{1}{2}} = r_i - \frac{r_i - r_{i-1}}{2} \quad \text{(d)}$$
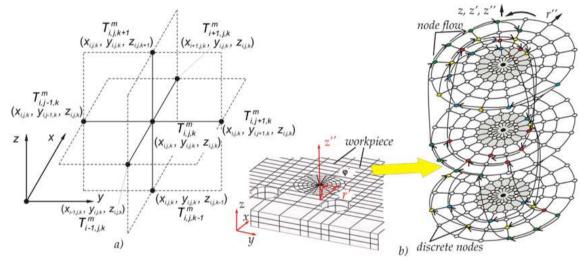
(37)

Figure 10. a) Discrete nodes with coordinates and temperatures, b) discretised space with a schematic of "node replacement and substitution" method [5]

3. Experimental procedure applied on aluminium alloy 2024 T351

The analytical model for estimating the amount of heat generated during FSW [5] is closely bound to the experimental research:

The analytical model gives realistic results only if some inputs into the model (axial force, torque, momentum of friction etc.) are obtained during realistic welding;

Validation of the analytical model and verification of gained results is possible only if some outputs from the model (e.g. numerically estimated temperature history of workpieces) are compared with the experimentally obtained results.

Such demands of the analytical model require a workplace with measuring equipment. Figure 11 gives a model of a realized workplace [5] where the welding of plates of Al 2024 T351 (some details given in Fig. 10, a) with the welding tool (given in Fig. 2, a) was performed.
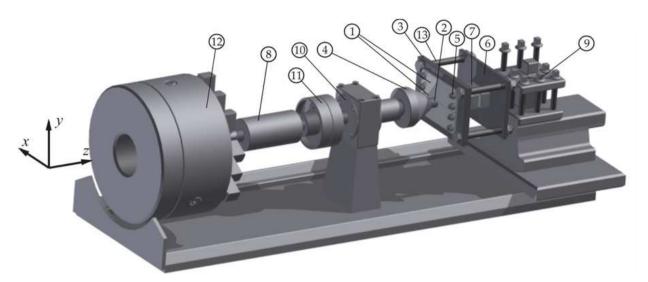
Figure 11. Workplace for FSW with measuring equipment: 1-workpiece, 2-welding tool, 3-anvil, 4-welding tool's spindle, 5-bolts, 6-backing plate, 7-force sensor, 8-torque sensor, 9-machine's tool rest, 10-bearing house, 11-clutch, 12-machine's spindle, 13-fundamental bolts
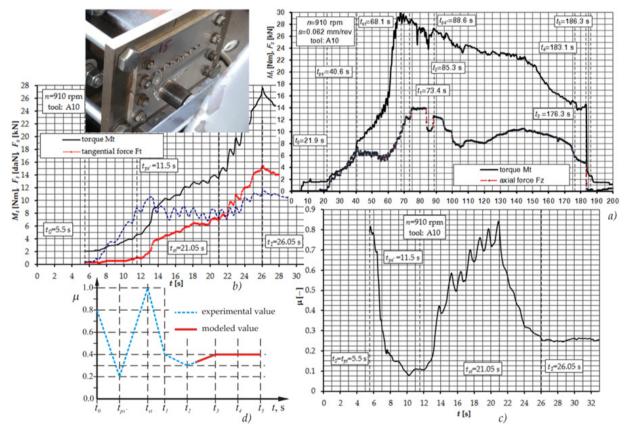

Figure 12. a) Typical diagram of measured torque and axial force, b) Typical diagram of measured torque, axial and tangential forces during FSW (plunging, first dwelling), c) Calculated friction coefficient, d) Modeled friction coefficient [5]

Welding was performed on a universal lathe with a horizontal operational axis (*z*-axis). Anvil, force sensor and backing plate are assembled and mounted on the machine's tool rest. Holes in the anvil (where fundamental bolts assemble force sensors) and the anvil and

backing plate are larger than the diameter of the bolts and allow for the axial translation of the force sensor and measurement of axial force. Workpieces (dimensions given in Fig. 9, a) are bolted to the anvil and tilted over the machine's tool rest at an angle of 1°. The welding tool and its spindle are clutched to the torque sensor that is mounted into machine's spindle. A rigid axial-radial bearing house between the clutch and the welding tool disables the transmission of axial and radial forces from the welding tool to the torque sensor and machine's spindle. Such a design provides the correct measuring of axial force on the welding tool. Second working/measuring configuration (given in Fig. 6) is used for measuring the momentum of friction, axial, and tangential force at the welding tool in order to estimate the experimental friction coefficient. The machines used for this measuring configuration are vertical milling machines. The anvil and workpieces are mounted on an axial bearing above the axial force sensor. The anvil carries a tangential friction pole engaged in measuring the tangential force delivered by the torque of the spindle. As previously mentioned, such a design of the measuring equipment provides usable results only for plunging and the first dwelling phases. An infrared camera was used for measuring both the configurations that were used to estimate the thermal history of workpieces and the welding tool.
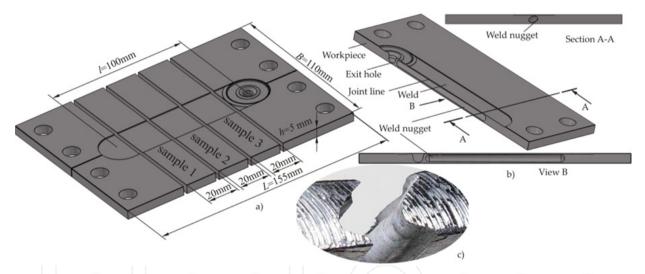

Figure 13. a) Schematic of sample extraction; b) Schematic of weld nugget's position; c) Tension sample destroyed at boundary of weld nugget

The experimental procedure of welding had three stages: to get familiar with the welding process, to get optimal technological parameters and to measure parameters necessary for the analytical model while creating qualitative welds [5]. Figure 12, a represents a typical diagram of torque and axial force measured during welding resulting in a qualitative weld.

Using a second measuring configuration, torque, axial and tangential force are obtained for numerous conditions. Figure 12, b shows a typical diagram of these parameters, obtained with optimal technological parameters. These values are used for estimating the experimental value of the friction coefficient (Fig. 12, c). However, since the proposed method gives limitedly usable values of the friction coefficient, based on experimental results, the friction coefficient is modeled for usage in the analytical model (Fig. 12, d).

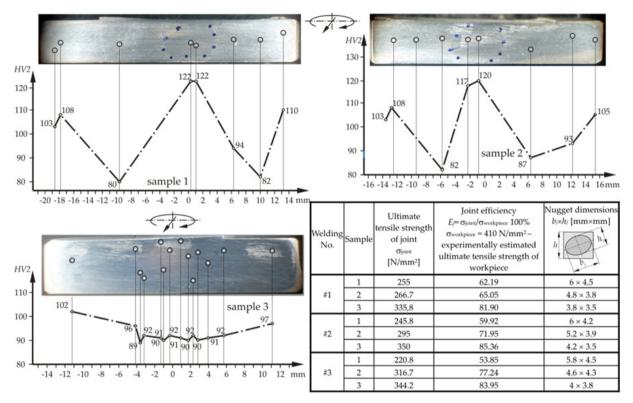| Welding No.	Sample	Ultimate tensile strength of joint σ_{joint} [N/mm²]	Joint efficiency $E_f = \sigma_{joint}/\sigma_{workpiece} \cdot 100\%$ $\sigma_{workpiece} = 410$ N/mm² – experimentally estimated ultimate tensile strength of workpiece	Nugget dimensions $b_j \times h_j$ [mm×mm]
#1	1	255	62.19	6 × 4.5
	2	266.7	65.05	4.8 × 3.8
	3	335,8	81.90	3.8 × 3.5
#2	1	245.8	59.92	6 × 4.2
	2	295	71.95	5.2 × 3.9
	3	350	85.36	4.2 × 3.5
#3	1	220.8	53.85	5.8 × 4.5
	2	316.7	77.24	4.6 × 4.3
	3	344.2	83.95	4 × 3.8

Figure 14. Hardness, joint (tensile) efficiency and observed dimensions of the welding nugget in samples 1, 2, 3 extracted from welded workpieces

In order to investigate the properties of welds (tensile and bending efficiency, hardness, metallic structure etc.), test samples were extracted from welded workpieces. Figure 13, a gives a schematic of the sample dimensions and positions of samples in workpieces. All welded joints used for sampling had a vortex-like structure of material called weld nugget, located along the joint line (Fig. 13, b). All tested samples (1-3) from all tested welds have a crack in the weld zone at the border of the nugget (Fig. 13, c).

Tested samples have shown a bending efficiency of about 12% (reaching a bending angle of about 11° while samples from parent material have reached an angle of about 89°). Results of joint (tensile) efficiency, the samples' hardness and the dimensions of the weld nugget in test samples are shown in Fig. 14.

4. Results and discussion

Whereas the experimentally obtained results included in analytical model makes use of some the necessary parameters affecting the heat generation process within FSW (contact pressure, shear stress etc.) and the amount of generated heat is relatively easily estimated, the numerical estimation of the temperature field of the wokpieces requires some computational time [5]. Experimentally estimated temperature can be easily inputted into analytical model in order to estimate the amount of heat generated during FSW and computational time can be significantly shorten. However, temperature change is the main product of heat generation and the verification of analytical model can be done via temperature comparison [56].
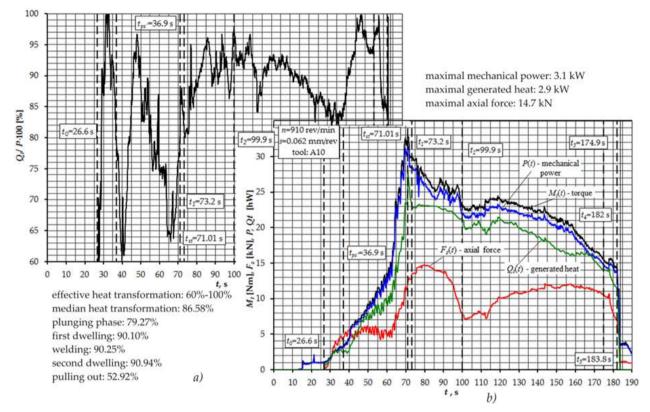
Figure 15. a) Effective heat transformation, b) Analytically estimated amount of generated heat [5, 56, 57]
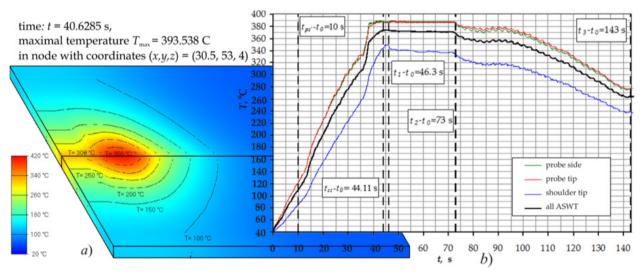

Figure 16. a) Numerically estimated temperature T of welding plates (rendered image); b) Median temperature of the material on contact with ASWT [5]

Figure 15, b gives the analytically estimated amount of generated heat during the welding of plates made of Al 2024 T351 (the dimensions of plates and technological parameters of the process are given in Fig. 9, a) with the welding tool with conned, threaded probe (given in Fig. 3, a). There were six repetitions of the welding procedure and the same number of applications of the analytical model. Characteristic moments of the process, operational technological parameters, values of measured axial force and torque delivered to the

welding tool are given in Fig. 15, b, as well. The ratio of generated heat and engaged mechanical power is effective heat transformation η_{Qef} (Fig. 15, a) and it varies between 60%-100% in this application. The median value of effective heat transformation is 86.58% while it reaches 90.25% during welding phase. The maximum generated heat is 2.9 kW, reached during the plunging phase (when the shoulder tip is involved in the welding process at t_{st}).
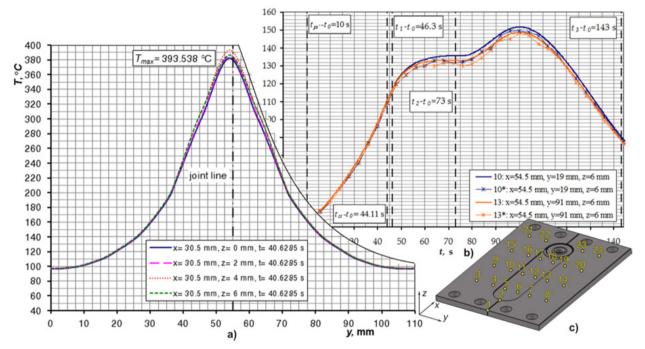

Figure 17. a) Temperature distribution in workpieces in plane normal to the joint line, b) temperature history (experimental and numerical) of specific discrete nodes, c) location of selected discrete nodes [56, 57]

Figure 16, a gives a rendered image of numerically estimated temperature in workpieces. Rendering is done for the moment the temperature reached maximal value – a few seconds before the tool shoulder was involved in the welding process. Figure 17, a gives the temperature distribution in a plane normal to the joint line for the same moment of time. The temperature peak is slightly dislocated from joint line to the advancing side of the weld. Analysis of heat generation required information about temperatures on contact between ASWT and the workpieces. Figure 16, b gives the median temperatures of all ASWT during the welding cycle. A comparison of the numerically and experimentally derived temperatures is done for 24 discrete points on the workpieces with adequate points from the numerical simulation (Fig. 17, c). Figure 17, b gives a diagram of both temperatures for two selected points. The largest difference between temperatures was about 11% in point 1 (absolute of 12°C) while other points had differences of 0.5-3.5% (absolute of 2-13°C) [5].

If the engaged mechanical power and generated heat are compared, it is clear that they have the same trend and notable changes in both are mostly connected with the characteristic moments of time. Mechanical power consumption and heat generation are more intense in the plunging and the first dwelling phases than in other phases. With a drop in the axial force (at the beginning of the first dwelling phase), torque drops as well, which results in

the stabilization of the heat generation process and a drop in the temperature of the workpieces. The welding process is always in a quasi-equilibrium state: increase in temperature lowers the generated heat, engages mechanical power and axial force; decreases of the temperature, and increases power consumption and heat generation (almost sinusoidal temperature character, Fig. 16, b). At the end of the first dwelling and the beginning of the welding phase, the system (tool-workpieces-anvil) has reached nearly the maximal observed temperatures. During the welding phase, the system constantly decreases the temperature – probably workpieces were "overheated" due to the long lasting first dwelling phase (t_{dw1}≈27 s). Power consumption and heat generation drop as well while axial force steadily rises until the moment when effective heat transformation reaches app. 85% (t≥150 s, Fig. 15, b) and axial force reaches a value of 11-12 kN. Analyzed results from tensile and hardness testing (Fig. 14), best distribution of hardness, smallest weld nugget and the most efficient welds of app. 80% are reached in test samples no. 3 – at the end of welding, where heat transformation has a value near 85%. Samples 1 have the worst joint efficiency (app. 55%), exhibiting W-shaped hardness distribution with great variation of hardness and largest weld nugget. Welding in the zone of samples 1 is performed at highest temperatures and with an effective heat transformation of app. 90% and the lowest axial force (7-9 kN).

5. Conclusions

The analytical model developed here utilizes analytical algebra, experimentally gathered data and numerical calculations to estimate how much of the mechanical power delivered to the welding tool is transformed into heat. The novel approach in the model focuses on the recognition of the active surfaces involved in welding, engagement of active surfaces during welding, recognition of dominant parameters involving heat generation and their estimation, recognition of mechanisms of heat generation and their utilization, and implementation of a new numerical model for defining the material flow around the welding tool. Experiments and temperature based validation of the model are done on Al 2024 T351 5 mm thick plates.

Results from the model have shown that 60-100% of the mechanical power of the welding tool transform into heat during FSW with a median of 86.58% in a complete welding cycle. The median value of heat transformation during welding is about 90% which is in agreement with previous results. Comparison of workpiece temperatures from numerical calculations and experiments has shown a maximal relative error of 11% (about 13°C) while the maximal temperature of workpieces reached a maximal temperature of app. 394°C (79% of Al 2024 T351 melting temperature).

Heat generation appeared to be extreme in the welding-procedure-dependent process: preheating of welding plates, derived by a long dwell of the welding tool at the beginning of the welding, has significant influence on heat generation and the quality of the welded joint. Too long dwelling "overheats" workpieces and the welding phase happens during continuous transient cooling. In such conditions, heat transformation is near (and above) 90%, joints have 50% tensile efficiency and a large weld nugget. For conditions of heat

transformation of app. 85%, joints reach app. 80% of tensile efficiency and have the smallest weld nugget. In both situations, it was necessary to have minimally 11kN of axial force to acquire a qualitative weld. If the optimal technological parameters of FSW and the welding tool are selected, heat management in FSW is of great importance for the quality of the weld. Due to the low bending efficiency of investigated welding, alloy 2024 T351 is legally considered to be a tough and a limitedly weldable alloy.

Author details

Miroslav Mijajlović* and Dragan Milčić
University of Niš, Faculty of Mechanical Engineering Niš, Serbia

6. References

[1] TWI, official web page: http://www.twi.co.uk/technologies/welding-coating-and-fabrication/friction-stir-welding/ (01.12.2011.)

[2] Thomas W M et al., Friction stir butt-welding, Int. Patent App., PCT/GB92/02203, 1991.

[3] Thomas W M et al., Friction stir butt welding, GB Patent App., No 9125978.8, 1995.

[4] Thomas W M et al., Friction stir butt welding, UP Patent, No 5 460 317, 1995.

[5] Mijajlović M. Investigation and Development of Analytical Model for Estimation of Amount of Heat Generated During FSW (in Serbian), Ph. D. thesis, Faculty of Mechanical Engineering Nis, University of Nis, Nis, Serbia, 2012.

[6] AWS D17.3/D17.3M:2010 Specification for FSW of Al Alloys for Aerospace Applications.

[7] ISO 25239: Friction stir welding – Aluminium, parts: 1-5, 2011.

[8] Maxwell JC. Theory of Heat. Dover Publications, Inc. ISBN 0-486-41735-2, 1871

[9] Ilić G. Radojković N. Stojanović I. Thermodynamics II: Basics of heat distribution (in Serbian), Vranje, Yugoslavia, 1996.

[10] Stamenković D. Djurdjanović M. Tribology of the Press Fit Joints (in Serbian), Faculty of Mechanical Engineering, Nis, Serbia, ISBN–86–80587–48–6, 2005.

[11] Djurdjanović M. Mijajlović M. Milčić D. Stamenković D. Heat Generation During Friction Stir Welding Process. Tribology in Industry. 2009; 31(1-2):8-14.

[12] Schmidt H.J. Hattel J.W. An analytical model for the heat generation in friction stir welding. Model. Simul. Mater. Sci. Eng. 2004; 12 (2004): 143–157.

[13] Lorrain O. Favierb V. Zahrounic H. Lawrjaniec D. Understanding the material flow path of friction stir welding process using unthreaded tools, Journal of Materials Processing Technology, 2010; 210 (2010): 603–609

[14] Nandan R. DebRoy T. Bhadeshia H.K.D.H. Recent advances in friction-stir welding – Process, weldment structure and properties. Progress in Mat. Sci. 2008; 53 (6): 980–1023.

[15] Chao YJ. Qi X. Thermal and thermo-mechanical modeling of friction stir welding of aluminum alloy 6061-T6, J. Mater. Proc. Mfg. Sci. 1998; 7 (1998): 215–233.

---

* Corresponding Author

[16] Frigaard O. Grong O. Modeling of the heat flow phenomena in friction stir welding of aluminum alloys, Paper presented at: INALCO '98. Proceedings of the Seventh International Conference on Joints in Aluminum, Cambridge, 15–17. April, 1998.

[17] Gould J.E. Feng Z. Heat flow model for friction stir welding of aluminum alloys, Journal of Material Processing and Manufacturing Science. 1998; 7(1998): 185-194.

[18] Russell M.J. Shercliff H.R. Analytical modeling of microstructure development in friction stir welding, Proceedings of the first International Symposium on Friction Stir Welding, Thousand Oaks, CA June 1999.

[19] Rosenthal D. The theory of moving sources of heat and its application to metal treatments [J]. Transaction ASME, 1946, 43(11): 849–866.

[20] Colegrove P. Painter M. Graham D. Miller, T. 3 Dimensional Flow and Thermal Modeling of the Friction Stir Welding Process, Proceedings of the Second International Symposium on Friction Stir Welding, June 26–28, 2000, Gothenburg, Sweden.

[21] Shercliff H.R. Colegrove P.A. Modelling of friction stir welding, Mathematical Modelling of Weld Phenomen. Maney Publishing, London, UK, 2002; 6(2002): 927-974.

[22] Khandkar M.Z.H. Khan J.A. Reynolds A.P. Prediction of temperature distribution and thermal history during friction stir welding: input torque based model. Science and Technology of Welding & Joining. 2003; 8(3): 165-174.

[23] Song M. Kovačević R. Thermal modeling of friction stir welding in a moving coordinate and its validation, Int. J. Machine Tool Manufacturing. 2003; 43 (6): 605–615.

[24] Hamilton C. Dymek S. Sommers A. A Thermal Model of Friction Stir Welding Applied to Sc-Modified Al-Zn-Mg-Cu Alloy Extrusions. International Journal of Machine Tools and Manufacture. 2008; 49 (2008): 230 – 238.

[25] Nandan, G.G. Roy, T.J. Lienert, T. Debroy, Three-dimensional heat and material flow during friction stir welding of mild steel, Acta Materialia. 2007; 55 (2007): 883–895.

[26] Ulysse, P. Three-dimensional Modelling of the Friction Stir-welding Process. International Journal of Machine Tools & Manufacture. 2002; 42(2002): 1549-1557.

[27] Steuwer A. Peel M. Withers, P.J. Dickerson, T.L. Shi, Q. Shercliff, H.R. Measurement and prediction of residual stresses in aluminium friction stir welds. Journal of Neutron Research. 2003; 11(2003): 267-272.

[28] Chao Y. J. Qi X. Tang W. Heat transfer in friction stir welding-experimental, and numerical studies. Transactions of the ASME. 2003; 125(2003): 138–145.

[29] Heurtier P. et al. Mechanical and thermal modelling of Friction Stir Welding Journal of Materials Processing Technology. 2006; 171 (2006): 348–357

[30] Santiago D.H et al. Numerical Modeling of Welded Joints by the Friction Stir Welding Process. Materials Research. 2004; 7(4): 569-574.

[31] Schmidt H. Hattel J. A Local Model for the Thermo-mechanical Conditions in Friction Stir Welding. Modelling and Simulation in Mat. Science and Eng. 2005; 13(2005): 77-93.

[32] Colligan KJ. Mishra RS. A conceptual model for the process variables related to heat generation in friction stir welding of aluminium. Scripta Mat. 2008; 58(2008): 327–331.

[33] Kalya P. Krishnamurthy K. Mishra RS. Baumann J. Specific Energy and Temperature Mechanistic Models for Friction Stir Processing of Al–F35. Presented at: 2007 TMS Annual Meeting Friction Stir Welding and Processing IV. Orlando, FL; 2007, pp. 113-126

[34] Kumar K. Kalyan C. Kaias SV. Srivatsan TS. An Investigation of Friction During Friction Stir Welding of Metallic Materials. Mat. and Man. Proc. 2009; 24(4): 438-445.

[35] Colligan K. Material Flow Behavior during Friction Stir Welding of Aluminum. Weld. J. Suppl. 1999; 78(7): 229s–237.

[36] Nandan R. et al. Improving reliability of heat transfer and materials flow calculations during friction stir welding of dissimilar aluminum alloys. Welding Journal, 2007; 86(10): 313S-322S.

[37] Ouyang JH. Kovačević R. Material Flow and Microstructure in the Friction Stir Butt Welds of the Same and Dissimilar Aluminum Alloys. The Journal of Materials Engineering and Performance. ASM International. 2002; 11(1): 51-63.

[38] Djurdjanović M. Tribology, Welding, Friction Welding. [unpublished materials used in studies at University of Nis, Faculty of Mechanical Engineering Nis, Serbia]. 2000-.

[39] Vukicevic M. Petrovic Z. Djuric S. Bjelic M. Oxy-fuel welding (in Serbian). Faculty of Mechanical Engineering. Kraljevo. Serbia. 2007

[40] Živković A. Influence of Friction Stir Welding Tool Geometry on Properties of Welded Joint of Alloys Al 2024 T351 (in Serbian) Ph. D. thesis. Faculty of Mechanical Engineering University of Belgrade, Belgrade, Serbia 2011.

[41] Rai R. De R. Bhadeshia HKDH. DebRoy T. Review: friction stir welding tools. Science and Technology of Welding and Joining. 2011; 16(4): 325-342.

[42] Mijajlović M. Milčić D. Anđelković B. Vukićević M. Bjelić M. Mathematical Model for Analytical Estimation of Generated Heat During Friction Stir Welding Part 1. Journal of Balkan Tribological Association. 2011; 17(2) 179-191.

[43] Mijajlović M. Milčić D. Anđelković B. Vukićević M. Bjelić M. Mathematical Model for Analytical Estimation of Generated Heat During Friction Stir Welding Part 2. Journal of Balkan Tribological Association. 2011; 17(3): 361-370

[44] Mijajlović M. et al. Study About Friction Coefficient Estimation in Friction Stir Welding. 2011; Presented at: Balkantrib 11, The 7th International Conference on Tribology, Proceedings, Thessaloniki, Greece, pp. 323-330.

[45] Hertz HR. On Contact Between Elastic Bodies(in German), Collected Works, 1(1885). Leipzig. Germany. 1895.

[46] Munisamy RL. Hills DA. Nowell D. The solution of the contact between a tilted circular rigid punch and an elastic half-space. Wear. 1995; 184(1995): 93-95.

[47] Levytsky VP. Interaction of Rigid Cylinder with Elastic Half-Space by Heat Generation on The Contact Area. Int. J. Engng. Sci. 1994; 32(11): 1693-1702.

[48] Galin LA. Contact Problems; The legacy of L.A. Galin. Series: Solid Mechanics and Its Applications (in Russian). Nauka. Moscow, Russia. 15(2008). 2008.

[49] Goryacheva I. Sadeghi F. Contact characteristics of a rolling/sliding cylinder and a viscoelastic layer bonded to an elastic substrate. Wear. 1995; 184(1995): 125-132.

[50] EN 573-3:2007, Al and Al alloys Part 3: Chemical composition and form of products.

[51] EN 485-2:2008-10, Al and Al alloys —Part 2: Mechanical properties.

[52] Metals Handbook: Properties and Selection: Non Ferrous Alloys and Special – Purpose Materials. 1992; 10(2). The American Society for Metals, ASM International, 1992

[53] ASM Aerospace Specification Metals Inc. Aluminium 2024 T351 Data Sheet. c2012 [Cited 27 August 2012]. Available from http://asm.matweb.com.

[54] Deng Z. Lovell MR. Tagavi KA. Influence of material properties and forming velocity on the interfacial slip characteristics of cross wedge rolling. Man. Science and Eng. 2001; 123(2001) :647–653, 2001.

[55] Khandkar H. Zahedul M. Khan J. Thermal modeling of overlap friction stir welding for Al-alloys, J. Mater. Process. Mfg Sci. 2001; 10 (2): 91–106.

[56] Milčić D. et al. Temperature Based Validation of the Analytical Model for Estimation of the Amount of Heat Generated During FSW. Thermal Science. In press. 2012.

[57] Mijajlović M. *et al*. Experimental Studies of the Parameters Affecting the Heat Generation in the Friction Stir Welding Process. Thermal Science. In press. 2012.